EUROPEAN ORGANIZATION FOR NUCLEAR RESEARCH

MEASUREMENT OF THE REACTIONS $\bar{p}p \to \bar{\Lambda}\Lambda$, $\bar{p}p \to \bar{\Lambda}\Sigma^0$ AND $\bar{p}p \to \bar{\Lambda}$ (MISSING MASS) AT 6 GeV

H. Becker*), G. Blanar*), W. Blum*), V. Chabaud**), J. De Groot***), H. Dietl*), J. Gallivan*), W. Kern†), E. Lorenz*), G. Lütjens*), G. Lutz*), W. Männer*), R. Mount**), D. Notz††), R. Richter*), U. Stierlin*) and M. Turala†††)

CERN-MPI Munich Collaboration

ABSTRACT

The reactions $\bar{p}p \to \bar{\Lambda}\Lambda$ and $\bar{p}p \to \bar{\Lambda}\Sigma^0$ have been measured at 6 GeV beam momentum in a wire-chamber experiment at the CERN PS with 25,500 and 10,800 events, respectively. We present cross-sections and polarizations, and compare our results with those of earlier experiments and with some theoretical predictions. For the reaction $\bar{p}p \to \bar{\Lambda}$ (missing mass) we present the polarization for those events accepted by our trigger.

Geneva - 20 April 1978

(Submitted to Nuclear Physics B)

---

*) Max Planck Institute for Physics, Munich, W. Germany.

**) CERN, Geneva, Switzerland.

***) Zeeman Laboratory, Amsterdam, Netherlands.

†) Permanent address: Southeastern University, Massachusetts, USA.

††) Now at: DESY, Hamburg, W. Germany.

†††) Permanent address: Institute of Nuclear Physics, Cracow, Poland.

1. INTRODUCTION

In this paper we present measurements of the total and differential cross-sections and polarizations of the reactions

$$\bar{p}p \to \bar{\Lambda}\Lambda \qquad (1)$$

and

$$\bar{p}p \to \bar{\Lambda}\Sigma^0 \ . \qquad (2)$$

These measurements were taken during the running of a wire-chamber experiment (S140) at the CERN PS. The primary aim of this experiment was to study the reactions $K^-p \to \Lambda_{forward}\pi^0$ and $K^-p \to \bar{\Lambda}_{forward}\eta$, with a view to measuring the πNN and ηNN coupling constants, and this work will be described elsewhere. Preliminary results of a study of $K^-p \to \bar{K}^0 n$ and $K^-p \to \bar{K}^0\Delta^0(1232)$, performed in the same experiment, have already been reported [1]. Our measurements of reactions (1) and (2) have a considerably greater statistical precision than previous work [2-9].

Reactions with final state Λ's or $\bar{\Lambda}$'s are particularly useful, as they allow an easy measurement of polarization. The $\bar{\Lambda}\Lambda$ final state also allows the measurement of spin correlations, although this was not possible in this experiment.

Reactions (1) and (2) are usually described in terms of Reggeized K^* and K^{**} exchange with absorptive corrections. We compare our measurements with the predictions of two such Regge models. Our data on the polarization in $\bar{p}p \to \bar{\Lambda}$(missing mass) are interesting, in spite of the limitation by our trigger to mainly neutral states, since they show large polarizations over most of the missing-mass spectrum.

2. EXPERIMENTAL DETAILS

2.1 The apparatus

Beam antiprotons at 6 GeV were measured by multiwire proportional chambers and Čerenkov counters and hit a hydrogen target. The products of the charged decays of fast $\bar{\Lambda}$'s were analysed by a wire-chamber spectrometer. The layout of the apparatus is shown in Fig. 1a, and the elements are described in more detail below.

2.1.1 Beam

The beam was a negative unseparated beam, produced at 5 mrad on a tungsten target by an external proton beam from the CERN PS. About 500,000 particles arrived at the experiment during the 300 msec burst, and the beam composition was 97.9% π^-, 1.4% K^- and 0.7% $\bar{p}$. The pions (and lighter particles) were rejected by two threshold Čerenkov counters, and discrimination between K^- and $\bar{p}$ was provided by a further threshold Čerenkov counter. Events flagged as $\bar{p}$ interactions contained fewer than 0.05% pion-induced events. The contamination by K^--induced events was larger (9%), but in the analysis this was greatly reduced by the selection of events with a forward $\bar{\Lambda}$. The momentum, angle, and position of the beam particles were measured by 1 mm pitch multiwire proportional chambers on either side of a 2 Tm bending magnet.

2.1.2 Target and target counters

The target region is shown in more detail in Fig. 1b. Two appendices of liquid hydrogen, each 0.45 m long and 35 mm in diameter, were placed along the beam with the circular 5 mm thick veto counters A1 and A2 placed immediately downstream of each. A 1 mm thick counter L was placed 0.5 m downstream of the A2 counter, so that the V^0 could be required to decay before the magnetic spectrometer. The window counter F was a shower counter, with a rectangular hole matching the magnet aperture.

2.1.3 Secondary particle spectrometer

This was based on a window-frame magnet with a bending power of 2 Tm and a field volume of 1.5 m long, 1.5 m wide, and 0.5 m high. On the upstream side of the magnet were twelve 2 mm pitch multiwire proportional chambers: four with vertical wires, four with wires at +30° to the vertical, and four with wires at -30° to the vertical. Downstream of the magnet were twelve wire spark chambers with magnetostrictive read-out. Each chamber had two wire planes of 1 mm pitch: one vertical and the other at either +31° or -31° to the vertical. The construction and performance of the spark chambers have already been described [10]. The chamber

assemblies upstream and downstream of the magnet were known as "arm 3" and "arm 4", respectively.

2.1.4 Trigger

The trigger was designed to detect events with only a V^0 in the forward direction. Hence the requirement was: a K^- or $\bar{p}$ beam signal -- either A1 or A2 (or both) -- giving no count, a signal from L and the first proportional chamber plane, and no signal from the window F. The trigger rate was about 10 per burst, and 9.8 million triggers were recorded in the period February to July 1976. A further 1.3 million triggers of various types were taken for calibration purposes.

2.2 Event reconstruction and fitting

Table 1 shows the numerical results of the selection of events by the reconstruction and fitting programs, and a brief description of this process is given below.

2.2.1 Geometrical reconstruction and event classes

The geometry program reconstructed track segments in space in each arm of the spectrometer. Events were retained if they had one beam track, if two of the arm-3 tracks made a fair V^0 vertex, and if either (or both) of these tracks could be matched to an arm-4 track.

At this point the events were divided into two classes

i) "one-legged events", where only one V^0 track was measured by the arm-4 spark chambers,

ii) "two-legged events", where both tracks were measured in arm 4.

As shown below, there were great differences in the quality of the differentiation between K^0, Λ, and $\bar{\Lambda}$, as well as in the acceptance, for the two classes. The missing-mass resolution for one-legged events was about 1.8 times poorer than that for two-legged events ($\sigma = 0.062$ GeV^2). For these reasons, the two classes were kept separate throughout the remaining analysis and only the final results were merged when they had been shown to be consistent.

2.2.2 Fitting and selection of events

The events were fitted to the hypothesis that the event corresponded, geometrically and kinematically, to the production and decay of a K^0, Λ, or $\bar{\Lambda}$. There was no kinematic constraint at the production vertex. One- and two-legged events were processed in the same way, except that the unknown momentum of the one-legged events reduced the number of constraints from three to two.

Table 2 shows the results of the fit for events where the K^- Čerenkov flag was not on. The discrimination between K^0, Λ, and $\bar{\Lambda}$ is very good for two-legged events, whereas for one-legged events it is poor, but can be improved somewhat by cuts. The third column of Table 2 shows the effects of a χ^2 probability cut of 5% combined with the removal of events with

$$|\theta \sin \alpha| < 0.025 ,$$

where θ is the V^0 opening angle, and α is the angle between the production and decay planes. These angle cuts remove events for which the momentum of the missing "leg" cannot be accurately determined. The increased numbers of unambiguous fits are due to the raising of the χ^2 probability threshold.

Arguments based on the charge symmetry of K^0 decays, and on the identity of the appearance of Λ and $\bar{\Lambda}$ decays after a reversal of the magnetic field, lead to an estimate that the $\bar{\Lambda}$ fits (ambiguous plus unambiguous) are 99.7% $\bar{\Lambda}$ for two-legged events. After the cuts mentioned above, one-legged events in the missing-mass^2 range 1.0 to 1.64 GeV^2 gave a $\bar{\Lambda}$ fit purity of 97.1%.

2.3 Acceptance corrections

Figure 2 shows the total acceptance of our apparatus as a function of t for reaction (1), calculated by the Monte Carlo method. The contributions of one- and two-legged events are also shown. The acceptance at small t was largely determined by the requirements that the production and decay vertex positions satisfied the trigger logic, and that the $\bar{\Lambda}$ decayed to $\bar{p}\pi^+$. At larger t, the acceptance was reduced by the limited aperture of the secondary particle spectrometer.

In addition to these large, but easily computed, effects there were important losses due to Λ decay products hitting the veto counters A1 and A2 (23% for $\bar{\Lambda}\Lambda$), and due to the interaction of the beam $\bar{p}$, the $\bar{\Lambda}$, or of the $\bar{\Lambda}$ decay products (total 23%). Other effects included vetoing by δ-rays hitting A1 or A2 (3%), π^+ decay (8%), and proportional chamber inefficiency in the path of the beam (2%). For reactions producing a Σ^0 or $\bar{\Sigma}^0$, the γ from the Σ decay could veto the event by hitting the F window (3% for $\bar{\Lambda}\Sigma^0$, 11% for $\bar{\Sigma}^0\Lambda$). The inclusion of $\bar{\Lambda}\Lambda$ spin correlations produced no detectable effects.

The drop in acceptance at very small t was due to a loss of events in the fitting program when the beam and $\bar{\Lambda}$ tracks were parallel within errors.

The acceptance calculation also applied the angle cuts for one-legged events and a cut on all events with track separation of less than 4.5 mm at the beginning of arm 3 as the 2 mm pitch proportional chambers did not allow these tracks to be reconstructed reliably.

The Monte Carlo calculation was checked by reading Monte Carlo generated events and data through the same program, which applied the same acceptance cuts as the Monte Carlo. Many distributions, including track densities in several planes perpendicular to the beam, and momentum distributions of the $\bar{\Lambda}$ decay products, were checked and good agreement was found.

2.4 Absolute normalization

After the exclusion of known periods of unstable conditions (17% of the data), the ratio

$$\frac{\text{observed } \bar{p}p \to \bar{\Lambda}X \text{ events}}{\text{expected events per microbarn}}$$

was calculated for each of 231 data tapes. Nine tapes gave ratios more than 5 standard deviations away from the mean and were rejected, leaving 80% of the data to be used for cross-section calculations.

For the cross-section calculation, only events flagged as having $\bar{p}$ beam were used, as these could be compared directly with the measured $\bar{p}$ flux, without the

need for an estimate of the accidental rate of the Čerenkov counter distinguishing K^- and $\bar{p}$. A correction for the 8% K^- contamination of the $\bar{p}$ flag was still necessary. Other losses and corrections not already included in the Monte Carlo are listed in Table 3.

3. RESULTS

3.1 Missing-mass distributions

Distributions of the square of the missing mass to the $\bar{\Lambda}$ for one- and two-legged events are shown in Fig. 3. In addition to the Λ and Σ^0, one sees clearly peaks at the $\Sigma(1385)/\Lambda(1405)$ and $\Lambda(1520)$ masses[2]. For both classes of events, the Λ and Σ^0 peaks are sufficiently well resolved that it is possible to extract $d\sigma/dt$ and polarization independently for the two reactions, given an adequate understanding of the background under the peaks.

3.1.1 $\bar{\Sigma}^0$ background calculation

Most of the background comes from $\bar{\Sigma}^0 \to \bar{\Lambda}\gamma$ decays, resulting from the reactions

$$\bar{p}p \to \bar{\Sigma}^0\Lambda \qquad (3)$$

and

$$\bar{p}p \to \bar{\Sigma}^0\Sigma^0 \ . \qquad (4)$$

Reactions (3) and (4) contribute two pedestals about 1.4 GeV^2 wide, starting near the squares of the Λ and Σ^0 masses, respectively. Since reaction (3) is the charge conjugate of reaction (2), we take

$$\frac{d\sigma}{dt}(\bar{p}p \to \bar{\Sigma}^0\Lambda) = \frac{d\sigma}{dt}(\bar{p}p \to \bar{\Lambda}\Sigma^0) \ .$$

And since the contribution of reaction (4) in the region of interest is only a few per cent, this background can be estimated by assuming :

$$\frac{d\sigma}{dt}(\bar{p}p \to \bar{\Sigma}^0\Sigma^0) \approx \frac{d\sigma}{dt}(\bar{p}p \to \bar{\Lambda}\Sigma^0) \times \frac{\sigma(\bar{p}p \to \bar{\Lambda}\Sigma^0)}{\sigma(\bar{p}p \to \bar{\Lambda}\Lambda)} \ .$$

An estimate of $d\sigma/dt$ for $\bar{p}p \to \bar{\Lambda}\Sigma^0$ was obtained by selecting two-legged events in the mass-squared range 1.37-1.51 GeV^2, and this was used to generate Monte Carlo events of reactions (3) and (4) using the above prescription. The final corrected $d\sigma/dt$ for $\bar{p}p \to \bar{\Lambda}\Sigma^0$ was sufficiently close to the first estimate that a further iteration was not needed.

3.1.2 Non-$\bar{\Sigma}^0$ background

After subtracting the $\bar{\Sigma}^0$ background calculated by the Monte Carlo, there remained the background arising from other sources such as $\bar{K}^0$ contamination of the $\bar{\Lambda}$ fits. This background was assumed to have the form $(a + bm^2) \times$ (number of $\bar{\Lambda}\Lambda + \bar{\Lambda}\Sigma^0$ events), and a and b were found by fitting this expression, together with peaks at the Λ and Σ^0 masses^2, to the missing-mass^2 spectrum for all t. The fits gave a background of 2% of the Λ peak height for one-legged events, and less than 1% for two-legged events.

The Λ and Σ^0 peaks, and the non-Σ^0 background fitted to the missing-mass^2 spectra are shown as dotted curves in Fig. 3, together with the $\bar{\Sigma}^0$ background calculated by Monte Carlo. The shape of the Λ and Σ peaks, calculated by the geometrical fitting program, was found to represent the data very well.

3.2 Differential cross-sections

The small variation of the missing-mass^2 resolution with t was predicted by the geometrical fitting program. Thus differential cross-sections could be determined by fitting the missing-mass^2 distribution in each range of t with only the numbers of $\bar{\Lambda}\Lambda$ and $\bar{\Lambda}\Sigma^0$ events as variables. The average χ^2 per degree of freedom for these fits was 1.2.

The results for one- and two-legged events were found to agree and were then merged to give the differential cross-sections shown in Fig. 4a ($\bar{p}p \to \bar{\Lambda}\Lambda$) and Fig. 4b ($\bar{p}p \to \bar{\Lambda}\Sigma^0$). The differential cross-sections are also given in Table 4. The errors shown are our estimate of contributions from all sources except the over-all normalization. The bin 0 to 0.005 GeV^2 has been corrected for the loss

of events whose beam and $\bar{\Lambda}$ tracks were parallel within errors, and the large error reflects the uncertainty of the correction. In the other bins, the uncertainty of the partition between Λ and Σ^0 contributes some 50% of the error. This contribution will be strongly correlated between neighbouring bins in t.

The differential cross-sections for both reactions give good fits to empirical functions of the form

$$ab\ e^{bt} + cd\ e^{dt} .$$

The results of these fits are given in Table 5. We find the forward peak to be somewhat sharper than the average of earlier experiments (mainly at lower energy). However, we confirm that the forward peak is significantly sharper in the $\bar{\Lambda}\Sigma^0$ channel than in the $\bar{\Lambda}\Lambda$ channel.

3.3 Total cross-sections

Integrating $d\sigma/dt$ from 0 to -1.0 GeV^2 gives total cross-sections of 40.5 ± 4.1 μb for $\bar{p}p \to \bar{\Lambda}\Lambda$ and 20.0 ± 2.1 μb for $\bar{p}p \to \bar{\Lambda}\Sigma^0$, where the normalization uncertainty is now included in the errors. Our empirical fits to $d\sigma/dt$ indicate that a further 0.9 (0.8) μb should be added to the $\bar{\Lambda}\Lambda$ ($\bar{\Lambda}\Sigma^0$) cross-sections to give total cross-sections integrated over all t of 41.4 ± 4.1 and 20.8 ± 2.1 μb for the two reactions. Figure 5 shows these points and earlier measurements plotted as a function of s. Our values are in good agreement with the trend of earlier data. Fits of functions proportional to s^n give values of n of -1.56 ± 0.12 for $\bar{\Lambda}\Lambda$, and -1.49 ± 0.29 for $\bar{\Lambda}\Sigma$. For $\bar{\Lambda}\Lambda$ we used all the data in Fig. 5a, whereas for $\bar{\Lambda}\Sigma$ we somewhat arbitrarily excluded from the fit the three points below 3.0 GeV, and even so the fit is rather poor.

The ratio of the cross-sections is predicted to be 1/3 by a simple SU(3) exchange model assuming the exchange of an octet in the t channel and pure F-type coupling [11]. The ratio is shown as a function of s in Fig. 5c, and appears to be significantly above this simple prediction away from the threshold region.

3.4 Polarization

The almost perfect symmetry of our apparatus under reflection in a horizontal median plane leads directly to the evenness of the acceptance as a function of $\cos \theta^*$, where θ^* is the angle between the $\bar{p}$ from $\bar{\Lambda}$ decay and the normal to the production plane in the $\bar{\Lambda}$ c.m.s. This in turn allows the calculation of polarization by the estimator

$$\alpha P = \frac{\Sigma \cos \theta^*}{\Sigma \cos^2 \theta^*} ,$$

with variance

$$\approx \frac{1}{\Sigma \cos^2 \theta^*} ,$$

where α is the $\bar{\Lambda}$ asymmetry parameter $\left(-0.647 \pm 0.014 \text{ [12]}\right)$. This expression does not involve the shape of the acceptance, and thus remains correct even if spin correlations have modified the shape, or even if there is an error (however unlikely this may be) in the Monte Carlo calculation.

To calculate polarizations using this prescription, data in the missing-mass^2 range 1.00 to 1.34 GeV^2 were treated as $\bar{\Lambda}\Lambda$ and data in the range 1.34 to 1.54 GeV^2 were treated as $\bar{\Lambda}\Sigma^0$. The mutual contamination was corrected algebraically, but the background from $\bar{\Sigma}^0\Lambda$ and $\bar{\Sigma}^0\Sigma^0$ could only be estimated by assuming a $\bar{\Sigma}^0$ polarization of +1 and -1 and increasing the errors on the measured points by the magnitude of the change produced. For most t bins this change was about ± 0.03 for $\bar{\Lambda}\Lambda$ and ± 0.05 for $\bar{\Lambda}\Sigma^0$. As for the differential cross-sections, polarization data for one- and two-legged events were merged after they had been seen to be consistent. The polarization for each reaction is shown as a function of $t_{min} - t$ in Fig. 6.

The most striking feature of the data for both reactions is the strong negative polarization*) for values of -t above 0.2. This has also been indicated

---

*) Negative polarization implies that the π^+ is found more often in the hemisphere opposite to beam $\times \bar{\Lambda}$.

by earlier measurements. For lower values of -t, our data are suggestive of a small positive polarization for reaction (2), whereas for reaction (1) there is no detectable positive swing.

3.5 $\bar{\Lambda}$ polarization as a function of missing mass

As stated above, the symmetry of our apparatus makes a complete understanding of the acceptance unnecessary for the calculation of polarization, although this is clearly not so for $d\sigma/dt$. We can thus present the $\bar{\Lambda}$ polarization as a function of t for a succession of missing-mass^2 ranges, and this is shown in Fig. 7. The value of these data is limited, as they are neither completely inclusive nor exclusive, but are rather for that subsample of the inclusive events $\bar{p}p \to \bar{\Lambda}X$ which produces no charged products in a forward cone averaging 25° half angle.

The ranges of missing mass^2 have been chosen to correspond approximately with the obvious structure of the spectrum. For completeness, the polarization in the Λ and Σ^0 regions is shown again in Figs. 7a and 7b, this time with no corrections for contamination. The polarization in the bumps near the masses of the $\Sigma(1385)$ and $\Lambda(1405)$ (Fig. 7d), and of the $\Lambda(1520)$ (Fig. 7f), is particularly interesting. The $\Sigma(1385)/\Lambda(1405)$ bump shows strong polarization similar to that in the Λ peak, whereas in the $\Lambda(1520)$ peak the effects are smaller. In all the missing-mass slices, the data are consistent with a substantial negative polarization in the t range -0.5 to -1.0 GeV^2.

4. DISCUSSION

As with most measurements in hadron physics, there is scant possibility that our data will immediately stimulate a great deepening of the understanding of the underlying dynamics. Appealing qualitative descriptions of such data as ours are given by models involving the Reggeized exchange of hadrons with the appropriate quantum numbers, in our case K, K^*, K^{**}, ... However, as is freely admitted by their proponents, such models require a heavy input of assumptions to attain any predictive power, after which the inevitable disagreements with

subsequent experiment can rarely be seen as fatal to any individual part of the model. A possible exception to this situation would be the unquestionable observation of strong spin correlations in $\bar{p}p \to \bar{\Lambda}\Lambda$ (particularly the coefficient C_{zz}), which Regge phenomenologists [13,14] would find exceedingly difficult to reproduce in their models. As already mentioned, our apparatus did not permit us to measure spin correlations.

With these limitations in mind it is instructive to compare our data on $\bar{p}p \to \bar{\Lambda}\Lambda$ and $\bar{p}p \to \bar{\Lambda}\Sigma^0$ with the predictions of two Regge-model fits to earlier data. Plaut [13] has fitted data on reactions 1, 2, 3, and 4 only with a model involving exchange-degenerate K^* and K^{**} exchange and absorption. The predictions for $d\sigma/dt$ for reactions (1) and (2), and polarization for reactions (1), are shown as solid curves on Figs. 4a, 4b, and 6. The predictions are actually for 5.7 GeV, but the normalization is, in any case, arbitrary, since the model fits were normalized to the 5.7 GeV data of Ref. 8.

The predictions do not agree particularly well with our data in either the differential cross-sections or polarization. However, it is interesting to note that the difference between the shapes of $d\sigma/dt$ for reactions (1) and (2) is quite adequately predicted.

Sadoulet [14] has investigated a less restricted approach, in which most of the available data on charge and hypercharge exchange were fitted to an exchange-degenerate Regge model with absorption. Whereas Plaut argued that the contribution to reactions (1), (2), (3), and (4), from K exchange, was negligible, Sadoulet incorporated K exchange in his fits, and showed that the effects produced were indeed very small. Polarizations were not fitted but were used as a check. The predictions for $d\sigma/dt$ and polarization for reaction (1) are shown as the dotted curves in Figs. 4a and 6. Again the predictions are actually for 5.7 GeV. The relatively poorer agreement with the data, as compared with the more specialized parametrization of Plaut, is hardly unexpected.

We have commented on the limitations of our data on $\bar{p}p \to \bar{\Lambda}$ (missing-mass). However, these data do indicate that large polarization effects, similar to those we have observed for $\bar{p}p \to \bar{\Lambda}\Lambda$ and $\bar{p}p \to \bar{\Lambda}\Sigma^0$, exist in reactions where higher mass states are produced together with the $\bar{\Lambda}$.

5. CONCLUSION

We have measured the total and differential cross-sections and polarizations of the reactions $\bar{p}p \to \bar{\Lambda}\Lambda$ and $\bar{p}p \to \bar{\Lambda}\Sigma^0$ with greater statistical precision than previous work. Our measurements of polarization in particular have made full use of the high statistics. Our results are consistent with earlier measurements, but the model predictions available to us seem, at best, to give only a qualitative description of the data.

We should like to thank all concerned with the operation of the CERN PS during this experiment, and the personnel of the workshops of MPI (Munich) who constructed much of the equipment. Miss H. Carstens and Miss G. Waltermann gave invaluable help with the analysis of the data.

REFERENCES

[1] H. Becker et al., Preliminary studies of a high statistics measurement of the differential cross-section for $K^-p \to \bar{K}^0 n$ and $K^-p \to \bar{K}^0 \Delta^0(1232)$ at 6 GeV, paper presented at the European Conference on Particle Physics, Budapest, Hungary, July 1977, and to be published.

[2] B. Musgrave et al., Nuovo Cimento 35 (1965) 735.

[3] C. Baltay et al., Phys. Rev. 140B (1965) 1027.

[4] C.Y. Chien et al., Phys. Rev. 152 (1966) 1171.

[5] J. Badier et al., Phys. Letters 25B (1967) 152.

[6] G.P. Fisher et al., Phys. Rev. 161 (1967) 1335.

[7] N. Kwak et al., Bull. Amer. Phys. Soc. 14 (1969) 24.

[8] H.W. Atherton et al., Phys. Letters 30B (1969) 494.

[9] H.W. Atherton et al., Nuclear Phys. B69 (1974) 1.

[10] G. Grayer et al., Nuclear Instrum. Methods 99 (1972) 579.

[11] K. Tanaka, Phys. Rev. 135B (1964) 1186.

[12] Review of particle properties, Rev. Mod. Phys. 48, No. 2, Part II (1976).

[13] G. Plaut, Nuclear Phys. B35 (1971) 221.

[14] B. Sadoulet, Nuclear Phys. B53 (1973) 135.

Table 1

Selection of events by the reconstruction and fitting programs

Sample	1 leg	2 legs
Triggers	9,758,626	
Poor running conditions	637,787	
Events sent to spark filter	9,120,839	
Undecodable events	1,442	
Too few/many*) beam sparks**)	186,554	
Too few/many*) secondary sparks**)	5,364,509	
Events sent to track filter	3,568,334	
Too few/many*) beam tracks	287,764	
Too few/many*) secondary tracks	1,393,300	
Events sent to topological filter	1,887,270	
No V^0 vertex	426,885	
No tracks pass spectrometer magnet	312,847	
One or two tracks pass spectrometer magnet	852,156	295,382
Fail crude reconstructibility tests	135,288	18,124
Sent to fitting program	716,868	277,276
Two arm 3-arm 4 match failures	-	635
One arm 3-arm 4 match failure (2 legs become 1 leg)	25,904	25,898
Geometric (+ momentum balance) fit tried	716,862	250,743
Failures	37,367	13,106
Kinematic fit tried	697,495	237,637
With K^- flag	526,137	183,521
Without K^- flag	171,358	54,116

*) The total loss due to rejection of events with too many sparks or tracks was 1.0%. We have assumed these events to be unwanted triggers.

**) We call coordinates from proportional or spark chambers "sparks".

Table 2

Results of the kinematic fit (for events without K^- beam flag)

	2 legs	1 leg	1 leg after cuts
Kinematic fits tried	54,116	171,358	149,368
Unique K^0 fits	12,361	23,959	23,977
Unique Λ fits	3,444	8,524	8,633
Unique $\bar{\Lambda}$ fits	31,022	49,625	51,853
K^0 and Λ fit	286	13,986	9,829
K^0 and $\bar{\Lambda}$ fit	1,696	52,264	36,495
Λ and $\bar{\Lambda}$ fit	0	415	128
All three fit	0	11,193	1,085
No fit	5,307	11,392	17,368

Table 3

Corrections used in the cross-section calculation

	Correction %	
	1 leg	2 legs
Trigger losses:		
A1 and A2 accidentals	3.0 ± 1.0	
Inefficiency of 1st proportional chamber	1.8 ± 1.8	
F accidentals	6.3 ± 2.0	
Imperfect target filling	5.0 ± 5.0	
Beam track reconstruction losses	10.0	
Pattern recognition losses in the secondary spectrometer	1.0 ± 1.0	
Miscellaneous losses in the fitting program	2.5 ± 1.0	0
χ^2 probability cut	5.0 ± 3.0	1.0 ± 0.5
Empty target effects Gain of	9.3 ± 1.6	

Table 4

Differential cross-sections

$t_{min} - t$ (GeV^2)	$\bar{p}p \to \bar{\Lambda}\Lambda$		$\bar{p}p \to \bar{\Lambda}\Sigma^0$	
	$d\sigma/dt$ ($\mu b/GeV^2$)	r.m.s. error ($\mu b/GeV^2$)	$d\sigma/dt$ ($\mu b/GeV^2$)	r.m.s. error ($\mu b/GeV^2$)
0.0025	353.8	115.8	155.8	51.8
0.0075	253.8	12.5	138.4	8.4
0.015	246.4	8.4	135.5	5.7
0.025	250.8	8.3	125.3	5.5
0.035	216.6	7.6	112.3	5.2
0.045	212.2	7.6	106.3	5.2
0.055	185.2	7.1	93.4	4.8
0.065	163.9	6.7	87.2	4.6
0.075	155.4	6.5	74.2	4.3
0.085	141.0	6.0	58.2	4.0
0.095	130.7	6.2	71.5	4.1
0.11	112.6	4.2	53.0	2.8
0.13	98.8	4.0	41.0	2.7
0.15	85.8	3.8	37.0	2.6
0.17	72.4	3.7	32.7	2.5
0.19	65.3	3.6	24.6	2.5
0.22	52.1	2.4	20.9	1.6
0.26	39.9	2.3	17.9	1.6
0.30	30.2	2.1	17.4	1.5
0.34	27.2	2.1	13.8	1.4
0.38	22.2	2.0	10.4	1.3
0.45	15.0	1.1	9.4	0.8
0.55	11.3	1.0	6.2	0.7
0.65	6.4	0.9	6.2	0.7
0.75	6.1	1.0	3.9	0.7
0.9	4.0	0.7	2.2	0.5
1.1	1.1	0.6	1.9	0.4
1.3	0.8	0.6	1.5	0.5
1.6	0.5	0.3		
t_{min}	0.015 GeV^2		0.023 GeV^2	

Table 5

Parameters of the empirical fits to $d\sigma/dt$

	a (μb)	b (GeV^{-2})	c (μb)	d (GeV^{-2})
$\bar{p}p \to \bar{\Lambda}\Lambda$	24.2 ± 2.2	10.1 ± 0.6	16.5 ± 2.1	3.0 ± 0.3
$\bar{p}p \to \bar{\Lambda}\Sigma^0$	10.4 ± 0.9	13.3 ± 1.0	10.6 ± 0.9	2.6 ± 0.3

Figure captions

Fig. 1 : a) Layout of the apparatus.

b) Detail of the target region and trigger counters.

Fig. 2 : Acceptance of the experiment as a function of t for the reaction $\bar{p}p \to \bar{\Lambda}\Lambda$, showing the contributions from one- and two-legged events.

Fig. 3 : Missing mass squared to the $\bar{\Lambda}$ for

a) one-legged events,

b) two-legged events;

with dashed curves showing the fitted contributions from $\bar{p}p \to \bar{\Lambda}\Lambda$, $\bar{p}p \to \bar{\Lambda}\Sigma^0$ and the non-$\bar{\Sigma}^0$ background, and a histogram showing the $\bar{\Sigma}^0$ background estimated by Monte Carlo.

Fig. 4 : Differential cross-sections $d\sigma/dt$. The solid curves are the predictions of Plaut [13]; the dashed curve is the prediction of Sadoulet [14], both at 5.7 GeV.

a) $\bar{p}p \to \bar{\Lambda}\Lambda$,

b) $\bar{p}p \to \bar{\Lambda}\Sigma^0$.

Fig. 5 : Total cross-sections for

a) $\bar{p}p \to \bar{\Lambda}\Lambda$ and

b) $\bar{p}p \to \bar{\Lambda}\Sigma^0$, plotted against s. The curves are fits of the form $\sigma = as^n$;

c) the ratio of the cross-sections compared with a simple SU(3) model prediction.

Fig. 6 : $\bar{\Lambda}$ polarizations.

a) $\bar{p}p \to \bar{\Lambda}\Lambda$ compared with the predictions of the Regge models of Plaut (solid) and Sadoulet (dashed).

b) $\bar{p}p \to \bar{\Lambda}\Sigma^0$.

Fig. 7 : $\bar{\Lambda}$ polarization in successive missing-mass^2 ranges.

C=Čerenkov Counter P=Proportional Chambers H_2 = Liquid Hydrogen a)

S=Spark Chambers Fe = Iron Shielding

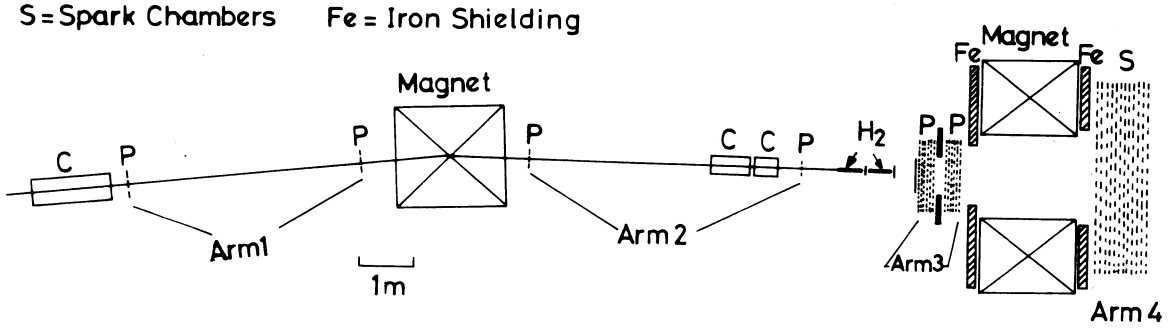

b)

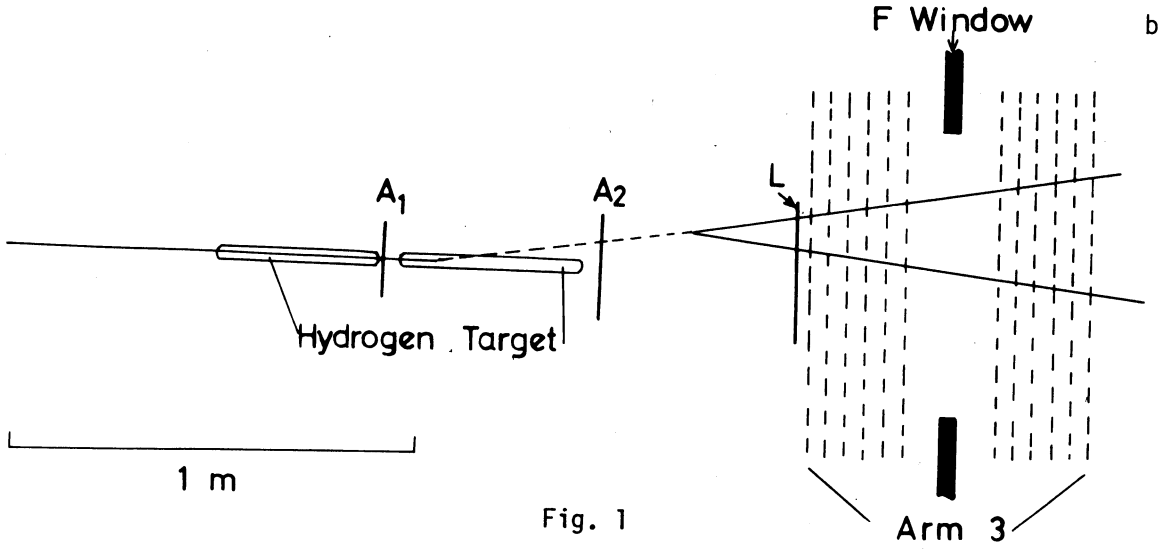

Fig. 1

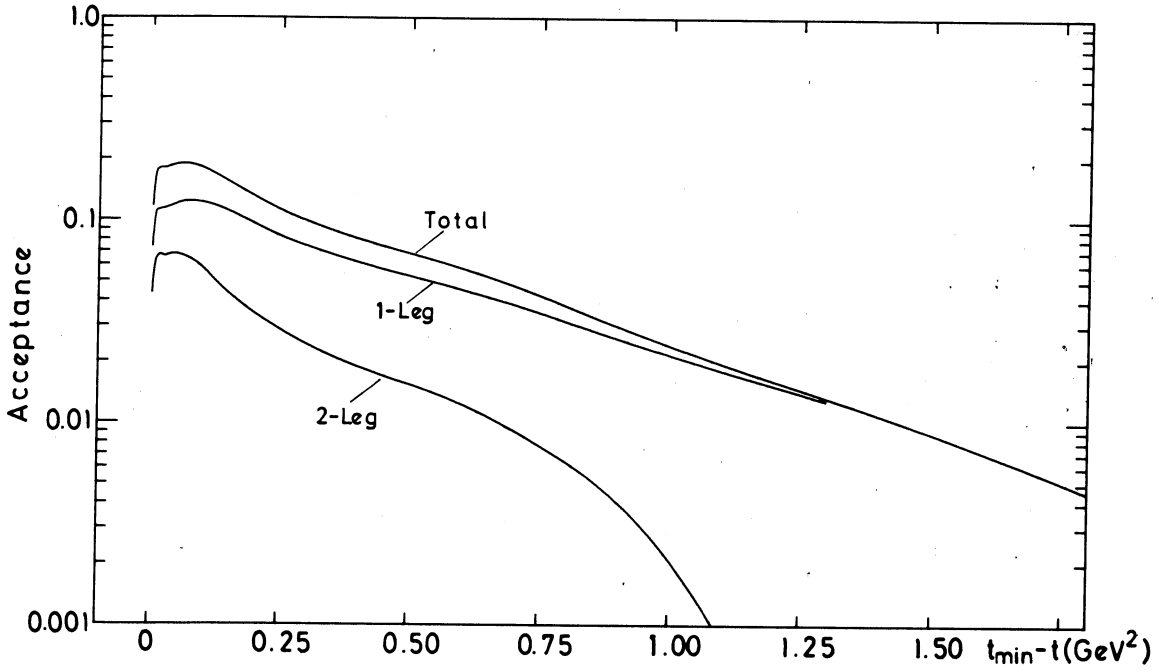

Fig. 2

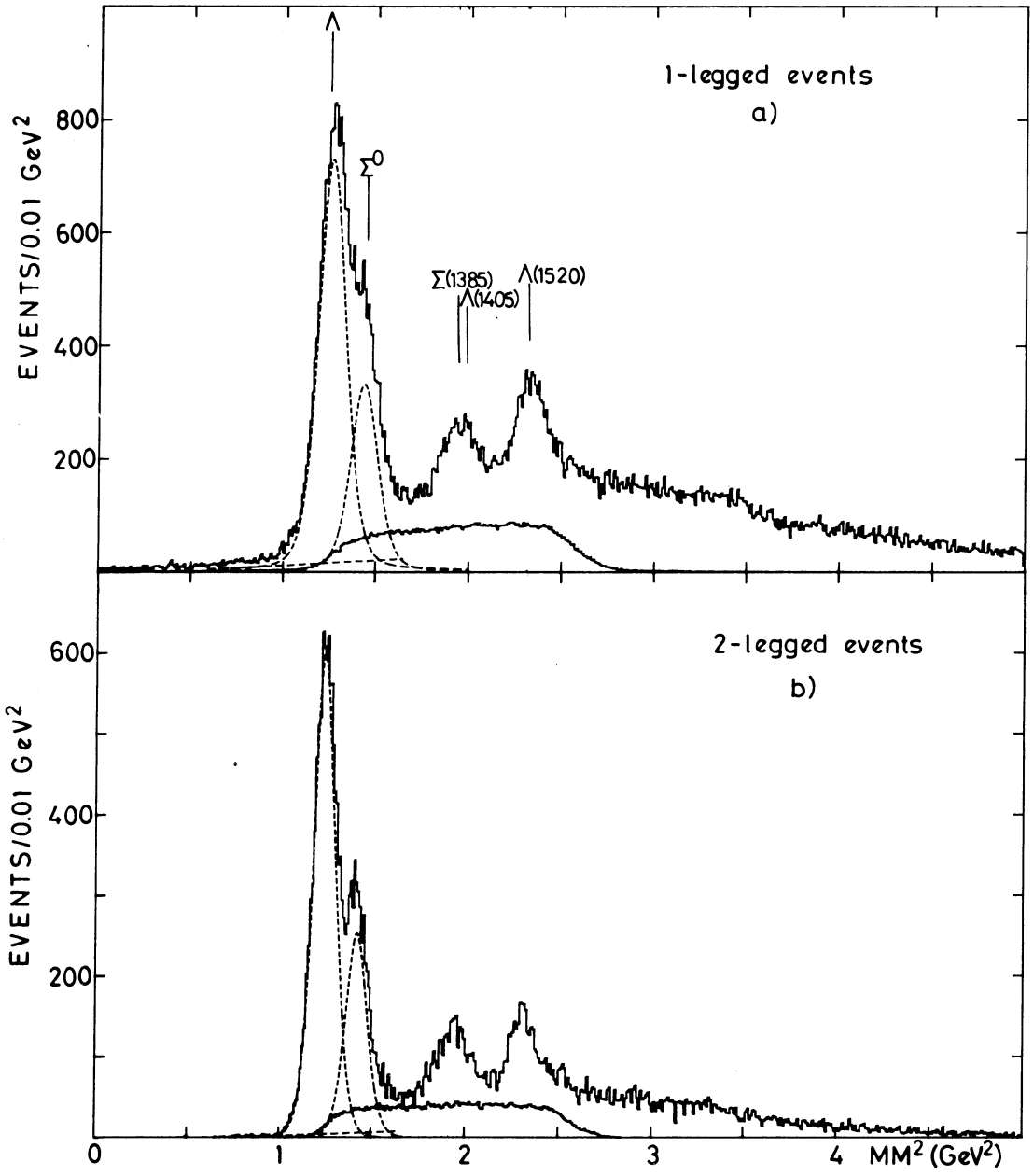
1-legged events
a)
Σ0
Σ(1385)
Λ(1405)
Λ(1520)
EVENTS/0.01 GeV2
800
600
400
200
2-legged events
b)
EVENTS/0.01 GeV2
600
400
200
0
1
2
3
4
MM2 (GeV2)

Fig. 3

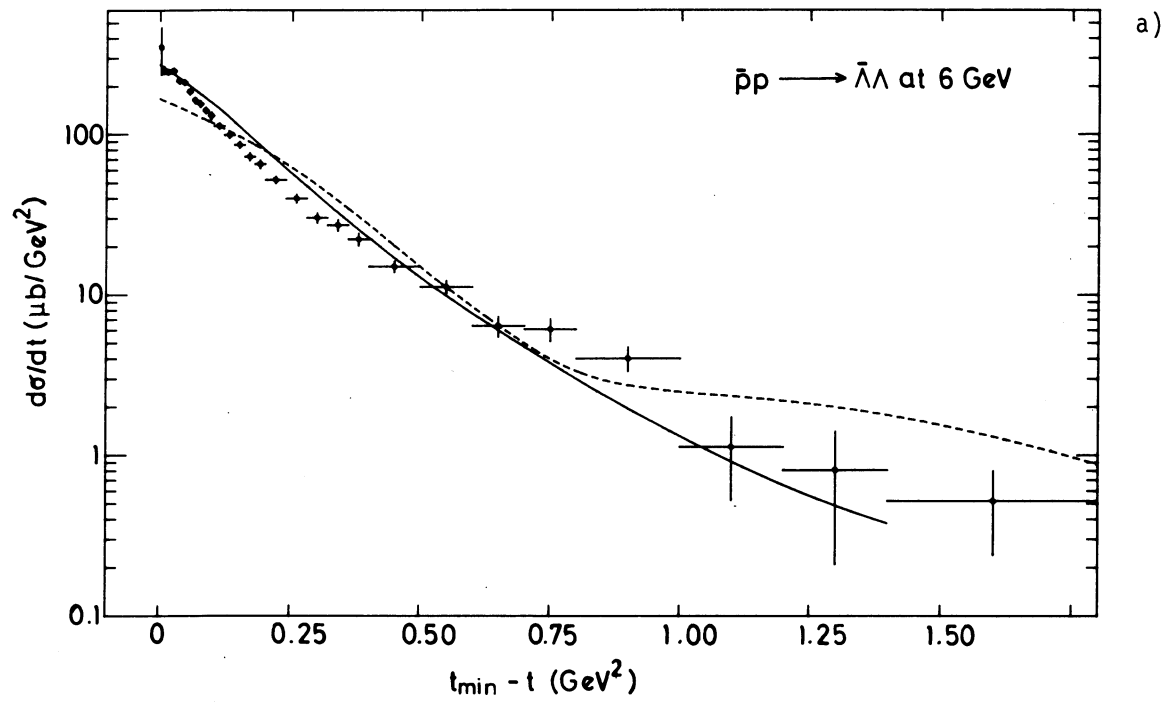
a)
$\bar{p}p \longrightarrow \bar{\Lambda}\Lambda$ at 6 GeV
$d\sigma/dt$ ($\mu b/GeV^2$)
100
10
1
0.1
0
0.25
0.50
0.75
1.00
1.25
1.50
$t_{min} - t$ (GeV^2)

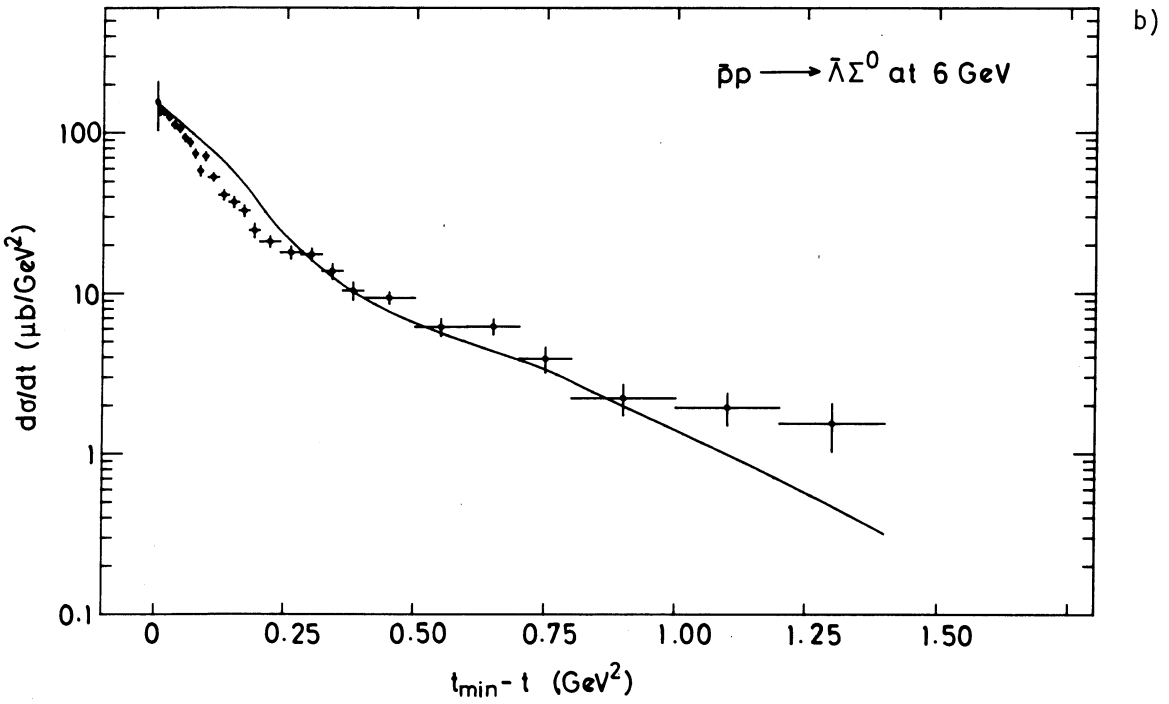
b)
$\bar{p}p \longrightarrow \bar{\Lambda}\Sigma^0$ at 6 GeV
$d\sigma/dt$ ($\mu b/GeV^2$)
100
10
1
0.1
0
0.25
0.50
0.75
1.00
1.25
1.50
$t_{min} - t$ (GeV^2)

Fig. 4

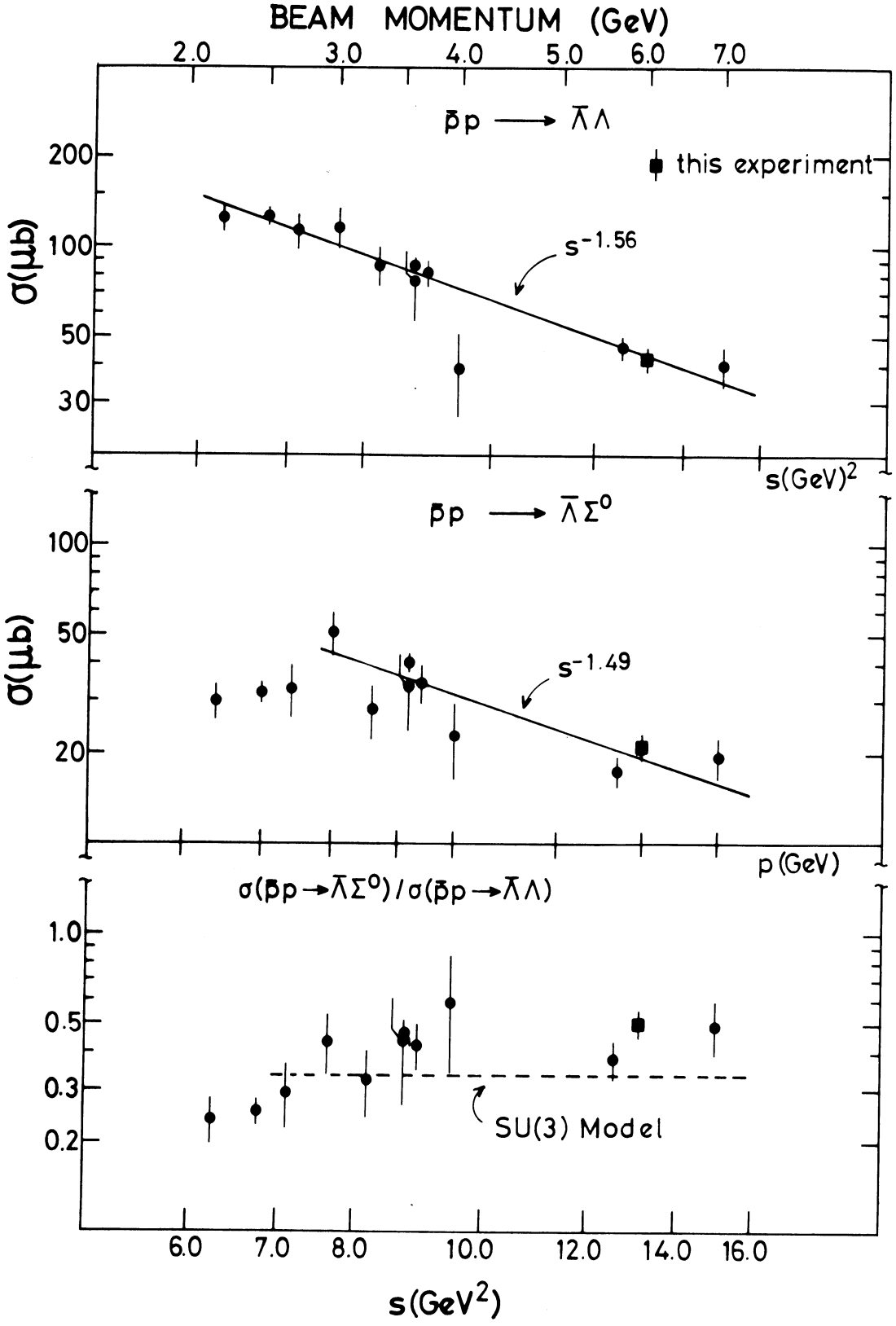
BEAM MOMENTUM (GeV)
2.0
3.0
4.0
5.0
6.0
7.0
$\bar{p}p \longrightarrow \bar{\Lambda}\Lambda$
this experiment
$s^{-1.56}$
200
100
50
30
σ(μb)
s(GeV)²
$\bar{p}p \longrightarrow \bar{\Lambda}\Sigma^0$
$s^{-1.49}$
100
50
20
σ(μb)
p (GeV)
$\sigma(\bar{p}p \to \bar{\Lambda}\Sigma^0)/\sigma(\bar{p}p \to \bar{\Lambda}\Lambda)$
1.0
0.5
0.3
0.2
SU(3) Model
6.0
7.0
8.0
10.0
12.0
14.0
16.0
s(GeV²)

Fig. 5

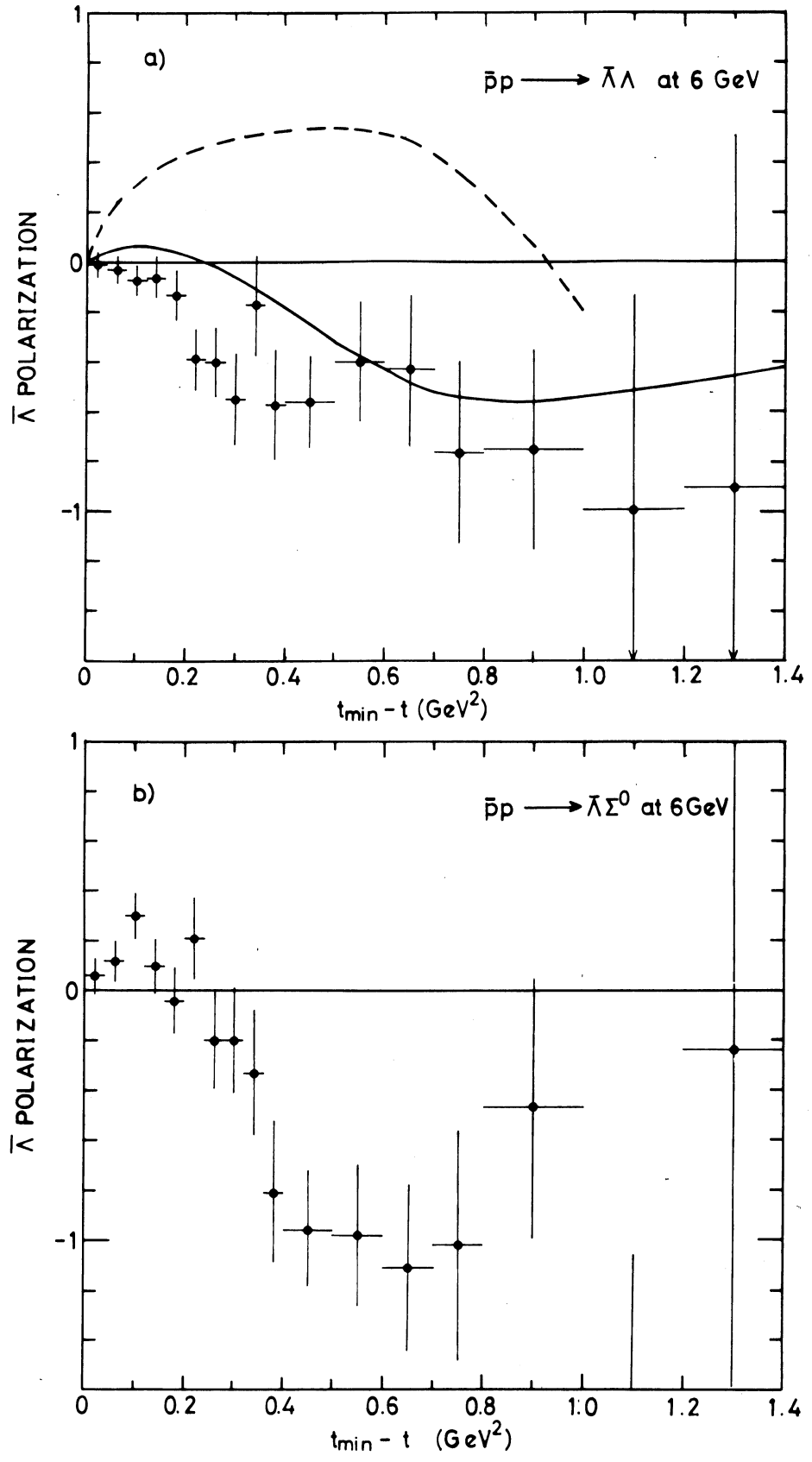
a)
$\bar{p}p \longrightarrow \bar{\Lambda}\Lambda$ at 6 GeV
$\bar{\Lambda}$ POLARIZATION
1
0
-1
0
0.2
0.4
0.6
0.8
1.0
1.2
1.4
$t_{min} - t$ (GeV^2)
b)
$\bar{p}p \longrightarrow \bar{\Lambda}\Sigma^0$ at 6GeV
$\bar{\Lambda}$ POLARIZATION
1
0
-1
0
0.2
0.4
0.6
0.8
1.0
1.2
1.4
$t_{min} - t$ (GeV^2)

Fig. 6

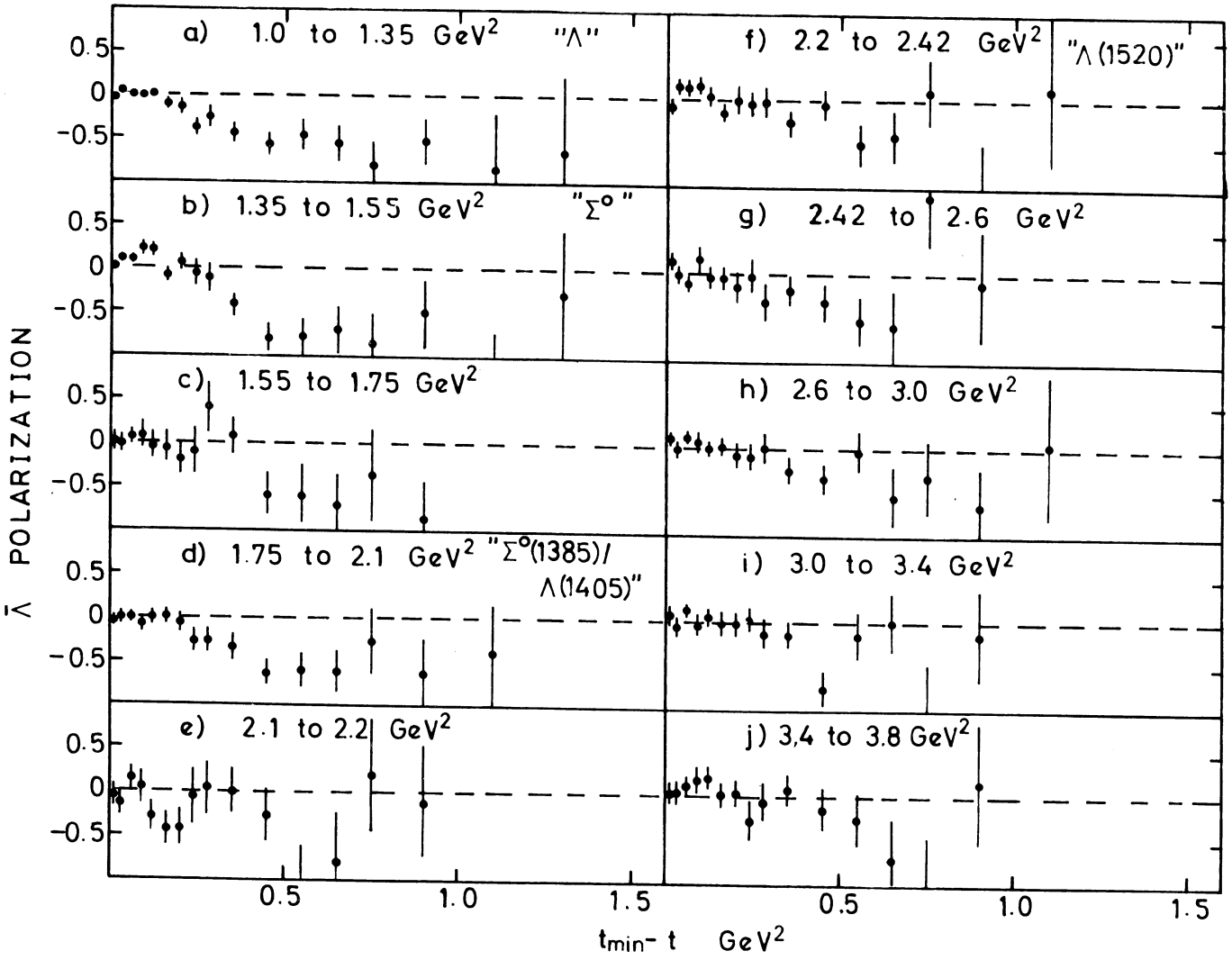
a) 1.0 to 1.35 GeV^2 "Λ"
b) 1.35 to 1.55 GeV^2 "Σ°"
c) 1.55 to 1.75 GeV^2
d) 1.75 to 2.1 GeV^2 "Σ°(1385)/ Λ(1405)"
e) 2.1 to 2.2 GeV^2
f) 2.2 to 2.42 GeV^2 "Λ(1520)"
g) 2.42 to 2.6 GeV^2
h) 2.6 to 3.0 GeV^2
i) 3.0 to 3.4 GeV^2
j) 3.4 to 3.8 GeV^2
$\bar{\Lambda}$ POLARIZATION
0.5
0
-0.5
1.0
1.5
$t_{min} - t$ GeV^2

Fig. 7